GEOPHYSICS, VOL. 75, NO. 3 (MAY-JUNE 2010); P. E123–E129, 15 FIGS.
10.1190/1.3383324

CO_2 velocity measurement and models for temperatures up to 200°C and pressures up to 100 MPa

De-Hua Han[1], Min Sun[1], and Micheal Batzle[2]

ABSTRACT

Studies on how the velocity of CO_2 is affected by temperature and pressure are important for understanding seismic properties of fluid and rock systems with a CO_2 component. We carried out laboratory experiments to investigate velocity of CO_2 in temperatures ranging from −10°C to 200°C and pressures ranging from 7 MPa to 100 MPa, in which CO_2 is in a liquid phase. The results show that under the above conditions, in general, the velocity of CO_2 increases as pressure increases and temperature decreases. Near the critical point (31.1°C and 7.38 MPa), the velocity of CO_2 reaches a minimum and has a complicated behavior with temperature and pressure conditions due to the CO_2 transition between gas and liquid phases. We also developed preliminary empirical models to calculate the velocity of CO_2 based on newly measured data.

INTRODUCTION

Recently, CO_2 has been considered a major factor in global warming as a result of the greenhouse effect. The increasing concentration of CO_2 in the atmosphere has been associated with human activity. The oil industry is a key contributor to controlling CO_2 emissions and with the environmental industry and the government, they work together to protect the Earth's environment. Extensive studies on the properties of CO_2 have been undertaken experimentally and theoretically to find ways to minimize its impact on the environment (Bachu, 2000; Benson et al., 2005). Consequently, CO_2 sequestration, injection, and storage are increasingly important strategies used to fight the global warming trend (Skov et al., 2002). However, strategic technology on such enormous scales of time, space, and economics is far from maturity. Many challenges remain unresolved (Bachu, 2000; Onishi et al., 2007; Sijacic et al., 2008), for example, where we try to store CO_2, how we control injected CO_2, how we ensure CO_2 will stay where it is, and so on.

The bottom line is that we need the capability to monitor CO_2 movement and distribution. Technologies developed in the energy industry to enhance oil recovery in different reservoirs, such as seismic monitoring of fluid movement and distribution (Wang et al., 1998; Xue et al., 2005), the influences of changes in in-situ pressure and temperature conditions, and monitoring of stress and fracture distribution and development, can play a crucial role in CO_2 sequestration operations (Lazaratos and Marion, 1997; Majer et al., 2006). Because fluids are the main target for monitoring, we have invested much effort to investigate seismic properties of hydrocarbon fluids (gas, oil, and brine) (Batzle and Wang, 1992; Han and Batzle, 2000a, 2000b). Carbon dioxide as a basic chemical compound has unique properties: It is a nontoxic, colorless, odorless, and nonflammable gas that is economically produced and purified. In the energy industry, CO_2 has been used as a major injection fluid (gas) because of its superior low viscosity, low surface tension, and high miscibility with oil.

Carbon dioxide also shows promise in displacing methane from coal and natural gas hydrates. It has not been a target of study as a globally harmful material subject to sequestration until recently. We need to investigate the seismic properties of CO_2 as a target fluid in the earth's system over a wide range of temperature and pressure conditions. Carbon dioxide has been injected into the ocean bottom at a depth of several thousands of meters with temperatures as low as 4°C and pressures as high as several tens of megapascals (Zhang, 2005). Carbon dioxide has been injected into subsurface reservoirs in which conditions could be above 200°C and 100 MPa. Near the surface, under pipeline conditions, the temperature of CO_2 is usually in the range of −20°C to 50°C and pressure is in the range of 5 MPa to 25 MPa (Folas et al., 2007). Carbon dioxide is usually in a liquid or supercritical phase under the above temperature and pressure conditions.

Many theoretical equations of state (EOS) have been developed for gases (e.g., Span and Wagner, 1996). Some of these relationships have been used to develop publicly available property calculation

Manuscript received by the Editor 2 May 2009; revised manuscript received 4 September 2009; published online 13 May 2010.
[1]University of Houston, Houston, Texas, U.S.A. E-mail: dhan@uh.edu; msun@mail.uh.edu.
[2]Colorado School of Mines, Golden, Colorado, U.S.A. E-mail: mbatzle@mines.edu.

software (Huber, 2007). However, CO_2 is such a unique gas with complex behavior that those equations are unable to accurately predict its thermodynamic properties (such as seismic velocity) (Batzle and Han, 1998), especially over the entire range of temperatures and pressures required for CO_2 operations. In addition, there are limited laboratory measurements of acoustic properties of CO_2 beyond 40 MPa.

In this paper, we present newly measured velocity data of CO_2 in a wide range of temperatures from $-10°C$ to $200°C$ and pressures from 7 MPa up to 100 MPa. We also develop preliminary empirical models to calculate the velocity of CO_2 based on measured data.

PHASE DIAGRAM OF CO_2

The pressure and temperature phase diagram of CO_2 shows three phases separated by phase boundaries between solid, liquid, gas, and supercritical fluid in conjunction with the triple point (0.518 MPa and $-56.6°C$) and the critical point (7.38 MPa and $31.1°C$), as shown in Figure 1 (after Shakhashiri, 2008). For CO_2 as an injected (storage) fluid under our measurement conditions, we mainly cover part of liquid- and supercritical liquid-phase regions as shown in Figure 1.

EXPERIMENTS

For our velocity measurements, we are using wave propagation in the megahertz range. Under our experimental conditions, CO_2 is in a fluid phase. Velocity depends on bulk modulus **K** and density ρ as

$$V_p = \sqrt{\frac{K}{\rho}}. \tag{1}$$

The bulk modulus here is the dynamic or adiabatic modulus. Compressibility values (inverse of bulk modulus) can be derived from the density behavior with pressure but these would be the static or isothermal values. The adiabatic and isothermal values can differ by around 50% in most regions but this difference increases substantially as the critical point is approached.

The measurement system consists of a test vessel, a transfer (storage) vessel, temperature control, and pressure control, as shown in Figure 2. The test vessel is composed of titanium and connected with

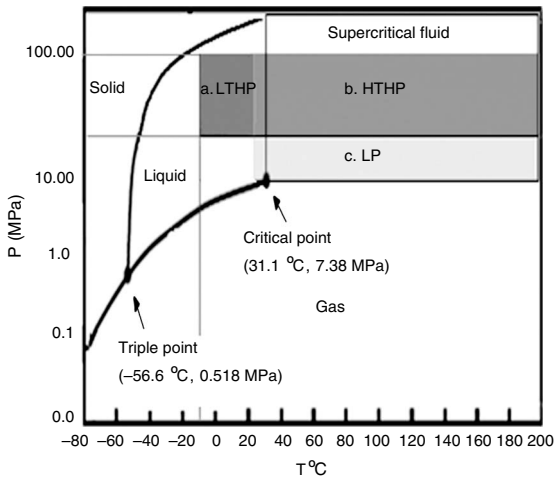

Figure 1. Phase diagram of CO_2 and experimental investigated areas: (a) LT and HP range; (b) HT and HP range; (c) LP range.

the transfer vessel. We use an ISCO digital pump (65D) to control the pressure of the transfer vessel and use a pressure transducer (Precise Sensors 6550) with 0.1% accuracy to measure the pressure of the CO_2 fluid in the test vessel. A silicon hot pad wrapped around the surface of the test vessel is used to heat the vessel. Temperature is controlled by a controller (Digi-Sense 2186-00) with a dual thermal couple system: one is placed on the outside surface of the test vessel to control the temperature of the hot pad and another is placed inside the sample chamber to monitor the temperature of CO_2 fluid to within $0.1°C$ accuracy. There are two acoustic transducers placed on both sides of the fluid-sample chamber. One is a transmitter and the other is a receiver. Velocity measurement depends on distance **L** (i.e., sample length) between the two transducers and traveltime t of acoustic wave between the transducers as

$$V = \frac{L}{t}. \tag{2}$$

Distance between the transducers varies slightly with variation of pressure and temperature. We use distilled water as a standard sample to calibrate the distance between the transducers as a function of pressure and temperature conditions. We apply the International Association for the Properties of Water and Steam — Industrial Formulation 1997 for the Thermodynamic Properties of Water and Steam (IAPWS-IF97; Wagner and Kruse, 1998) and the Fluid Application Geophysics program (FLAG program — a computer program developed by the Fluids/DHI consortium) as standard for the velocity of distilled water. In this way, the calibrated distance between the transducers is known at a given condition and velocity depends only on measured traveltime. This method is suitable for a stable system and high pressure and temperature measurement. However, we need to regularly check the calibration.

In an alternative technique, we use an acoustic probe to measure velocity directly. We apply a micrometer to move one transducer (with a limit of the sample pressure < 2000 psi) and measure distance change (ΔL) and traveltime change (Δt). In this way, velocity can be calculated directly as

$$V' = \frac{\Delta L}{\Delta t}. \tag{3}$$

We compare velocity V' with velocity V to calibrate the distance between the transducers. In the region near the critical point, we must use a different set of transducers and a resonant method to measure the extremely attenuated signal and low velocity. Considering controlled pressure and temperature conditions, the accuracy of ve-

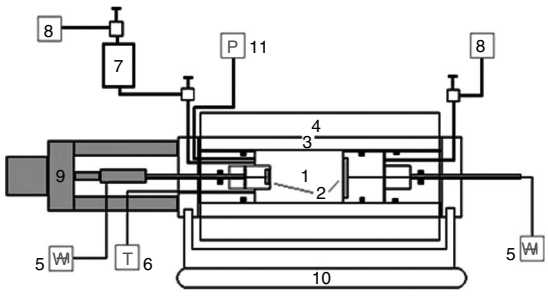

Figure 2. Schematic experimental setup: (1) fluid sample; (2) transducers; (3) sample vessel; (4) temperature controller; (5) scope; (6) temperature indicator; (7) CO_2 storage vessel; (8) digital pump; (9) micrometer; (10) system holder; (11) pressure indicator.

locity measurement of the CO_2 sample is better than 0.5%. Velocity data on the CO_2 sample are measured using an acoustic system consisting of a Pulser-receiver (Panametric 5055PR) and a LeCroy digital oscilloscope (WaveSurfer 42Xs). Although waveforms change with temperature, the first arrival is always distinct, as seen in Figure 3. All waveforms were recorded in the scope. We can pick the first arrival accurately and systematically with cross references of different waveforms in the same time base.

Considering different behaviors of CO_2 velocity in the wide range of temperature and pressure and different experiment set-ups, we need to separate the region of interest into three parts, as shown in Figure 1:

1) Low temperature (LT) and high-pressure (HP) range within the CO_2 liquid phase: $-10°C \leq T \leq 20°C$ and 20 MPa $\leq P \leq$ 100 MPa. Here we use a cooling bath to control the temperature of the vessel containing the CO_2 sample.
2) High temperature (HT) and HP range within the CO_2 supercritical fluid: $25°C < T \leq 200°C$ and 20 MPa $\leq P \leq$ 100 MPa. We use a simple heating pad to control the temperature of the CO_2 sample.
3) Low pressure (LP) range near the critical point of CO_2: 7 MPa $< P <$ 20 MPa.

Near the critical point (31.1 °C and 7.38 MPa), CO_2 is in a transition phase between liquid and gas. Its properties change drastically. The acoustic velocity decreases and nears zero as the critical point is approached (see, for example, Walas, 1985). We also apply much denser sampling in pressure (1 MPa interval) and temperature (5 °C interval) to examine in detail the velocity of CO_2 at the phase transition between liquid and gas.

In our measurements, we used industry-grade CO_2 (provided by Matheson Tri-Gas®) of 99.5% purity for measurement. In the earth, CO_2 will occupy the pore space with other fluids such as water or hydrocarbons. These compounds, when mixed with CO_2, can alter its properties substantially. The behavior of such mixtures is important but beyond the scope of this paper.

MEASURED RESULTS AND DISCUSSION

We present measured data in the following three parts.

Velocity of CO_2 in the LT and HP range

Low temperature (LT) means below room temperature (-10 to 20 °C) and HP ranges from 20 MPa to 100 MPa, as shown in Figure 1. Here, CO_2 is in a liquid form. Velocity data measured in the LT and HP range are shown in Figure 4. The velocity increases as pressure increases at a given constant temperature and decreases as temperature increases at a given constant pressure. We also observed that the gradient of velocity with respect to pressure gradually reduces with increasing pressure and decreasing temperature (larger pressure effect at a higher temperature and a larger temperature effect at a lower pressure), as indicated in Figure 4. However, the influence of the temperature effect to reduce velocity decreases with increasing temperature. According to equation 1, because the bulk modulus and density are functions of temperature and pressure, the resulting velocity change will depend on the competing relative change between bulk modulus and density. When the temperature remains constant, the increase of the pressure requires that more molecules be packed in a unit volume. This decreases the distance between molecules and causes an increase in density. The repulsive force between molecules in a liquid phase follows a nonlinear relationship with distance rather than a simple linear relationship, as in Hooke's law. When the liquid is compressed, the relative increase of the bulk modulus is greater than the relative increase of density, resulting in a velocity increase with a pressure increase.

A similar analysis tells us that increasing temperature at constant pressure will cause a relatively larger decrease in the bulk modulus than in density, thus, resulting in a decrease in velocity (Figure 5). The temperature effect on the decrease of velocity shows a trend to increase with decreasing pressure, especially at a pressure of 20 MPa, as shown in Figure 5. Carbon dioxide as an LP liquid is less confined and temperature shows a greater effect in reducing CO_2 velocity. Overall, we can summarize that the velocity data of the CO_2 liquid in LT and HP conditions is typical of a liquid.

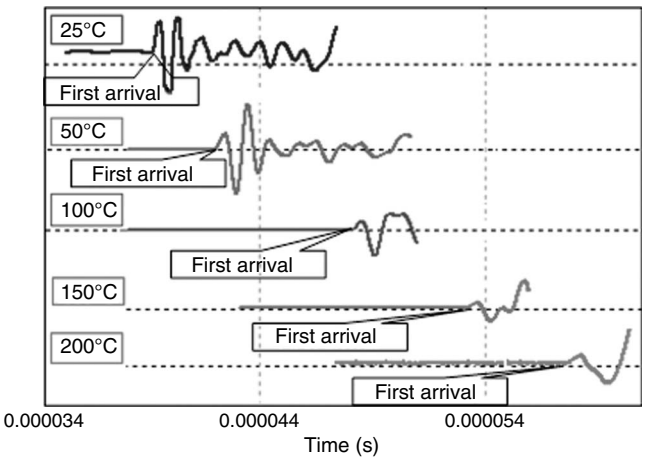

Figure 3. Waveforms of transmission P-wave received at pressure P = 100 MPa for different temperatures from 25 °C to 200 °C.

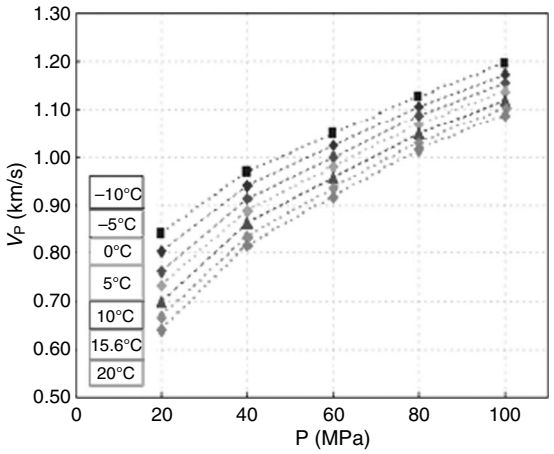

Figure 4. Measured velocities of CO_2 as a function of pressure P for different temperatures from 20 °C to −10 °C.

Velocity properties in the HT and HP range

Here HT means higher than room temperature (25–200°C). The examined pressure range is high (HP), from 20 MPa to 100 MPa. According to the phase diagram in Figure 1, CO_2 in this range is in a supercritical fluid phase.

Measured velocity data are shown in Figure 6. Similar to velocity data measured at an LT and HP range, the velocity of CO_2 in an HT and HP range increases as pressure increases at constant temperature and decreases as temperature increases at constant pressure. However, the temperature effect becomes complicated, as shown in Figure 7. At HP (>40 MPa), velocity of CO_2 decreases with increasing temperature in a monotonic manner but as pressure is lowered the dependence on temperature decreases. Eventually, at lower pressure and elevated temperature (the 20 MPa line in Figure 7), the velocity increases with increasing temperature. This type of temperature dependence is more typical of light gases. Thus, in this supercritical region, we begin to see the transition from liquid-like to gas-like behavior.

Velocity of CO_2 around the critical point

We also measured the CO_2 velocity near the critical point. Properties of CO_2 as a supercritical fluid are very sensitive to temperature and pressure as we approach the critical point (Walas, 1985). A very small drop in pressure can significantly change the phase state of CO_2 from liquid-like to gas-like. Remember that a passing acoustic wave is a small perturbation in pressure. Near the critical point, the molecules transition between liquid- and gas-like phases, resulting in rapid density change, decrease of velocity, and increase of wave attenuation. Therefore, we must apply a different measurement setup and much finer measurement intervals around the critical point. For temperatures from 25°C to 45°C, we use a 5°C interval and for pressures from 7 MPa to 13 MPa we use a 1 MPa interval.

As shown in Figure 8, the top two curves with temperatures of 25°C and 30°C (below the critical point temperature of 31.1°C) exhibit the typical liquid velocity-pressure relationship. However, when the temperature approaches and then exceeds the critical temperature (velocity data measured at 35°C, 40°C, and 45°C), the velocity-pressure relationship can be clearly separated into a gas-like regime and a liquid-like regime with minimum velocity between these two regimes. With decreasing pressure, CO_2 velocities in the liquid regime tend to decrease to a minimum due to a drastic decrease in modulus near the critical point and then to increase because density decreases drastically as CO_2 transitions from a liquid phase to a gas phase. The transition between the two regimes approximate-

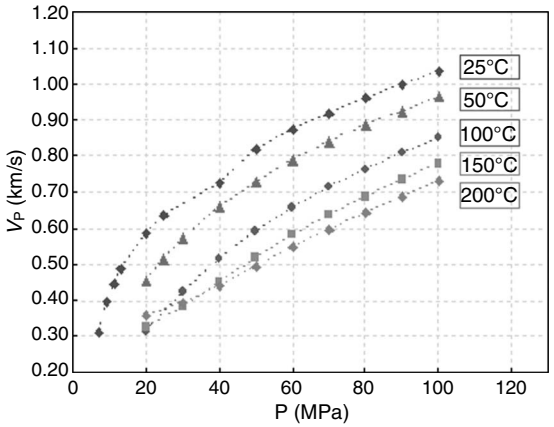

Figure 6. Measured velocities of CO_2 as a function of pressure P for different temperatures from 25°C to 200°C.

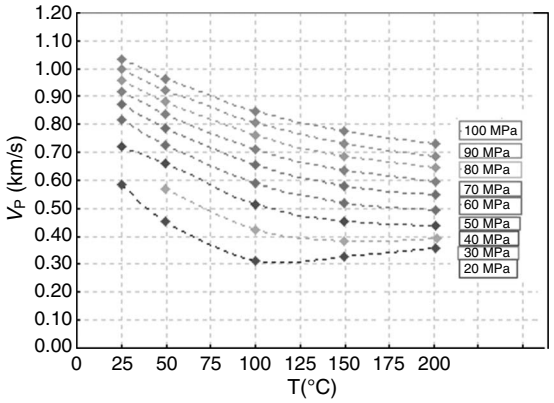

Figure 7. Measured velocities of CO_2 as a function of temperature T for different pressures from 20 MPa to 100 MPa.

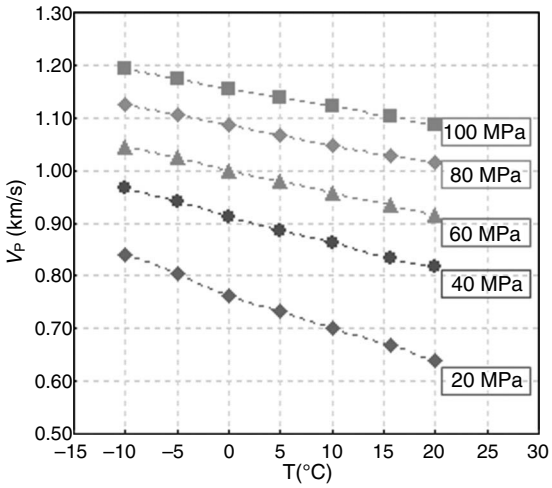

Figure 5. Measured velocities of CO_2 as a function of temperature T for different pressures from 20 MPa to 100 MPa.

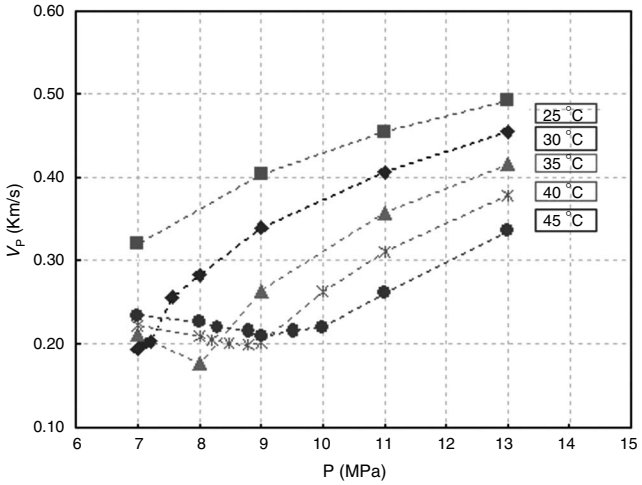

Figure 8. Measured velocities of CO_2 as a function of pressure P for the range near the CO_2 critical point.

ly corresponds to the CO_2 critical point pressure of 7.38 MPa. We also observe similar complicated temperature effects on velocities of CO_2 near the critical point (Figure 9). Thus, although we can reside in a single-phase supercritical state, behavior can be either liquid-like (HP) or gas-like (LP). For CO_2 in a liquid-like state, velocities will decrease with increasing temperature but the opposite is true for CO_2 in a gas-like state. High pressure tends to drive CO_2 to be a liquid whereas HT tends to drive CO_2 to be a gas. Velocities of CO_2 are determined by balanced temperature and pressure effects, especially near the critical point.

EMPIRICAL MODELS

Based on our three measured groups of data that cover wide ranges of pressures (7–100 MPa) and temperatures (−10–200 °C), we took several approaches to describe the velocity of CO_2. Initially, this included examining published models and then comparing them to the EOS for CO_2 (Duan et al., 1992; Span and Wagner, 1996; Batzle and Han, 1998).

We found that these model results either do not fit well with measured data or are too complicated for application; therefore, we developed empirical models. Because of the complexity near the critical point, we have not yet obtained a simple, accurate, unified empirical model for the three groups of data. However, here we present three empirical models to describe velocities of CO_2 valid under restricted temperature and pressure ranges.

CO_2 velocity model (LTHP) for the LT and HP range

Based on experimental results, the following polynomial model is suitable to describe CO_2 velocity as a function of temperature and pressure for this range:

$$V_p = a + bT + cT^2 + dP + eP^2 + fTP, \tag{4}$$

where $a = 0.61571$, $b = -0.00709$, $c = 0.00002$, $d = 0.00833$, $e = -0.00003$, $f = 0.00004$, V_P is in kilometers per second, T in degrees Celsius, and P in megapascals.

The comparison of calculated CO_2 velocities with measured data is shown in Figure 10. The model correctly matches the CO_2 velocity in the temperature and pressure range ($-10\,°C \le T \le 20\,°C$ and 20 MPa $\le P \le$ 100 MPa) to within an error of 0.7%.

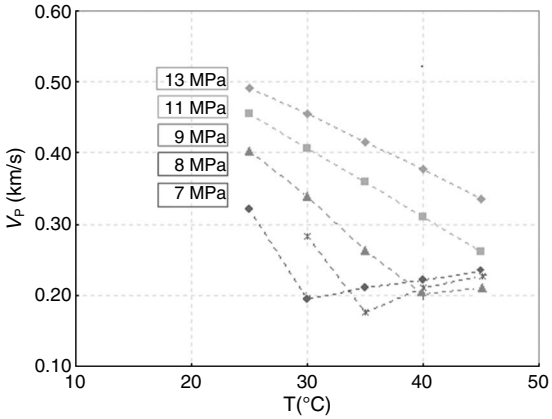

Figure 9. Measured velocities of CO_2 as a function of temperature T for the range near the CO_2 critical point.

CO_2 velocity model (HTHP) for the HT and HP range

We can use the following model for the HT and HP range:

$$V_p = (1 - W_f)V_{lp} + W_f V_{hp}, \tag{5}$$

where

$$W_f = \frac{W_{f1} + |W_{f1}|}{2(0.5 + |W_{f1}|)}, \tag{6}$$

$$V_{lp} = 150 + 120T_{pr} - [9 + 175(1.5 - T_{pr})^2]P_{pr}, \tag{7}$$

$$V_{hp} = 45 + 600(a - T_{pr})^3 + 246|P_{pr} - S_{hp}|^{0.44}, \tag{8}$$

and

$$W_{f1} = (P_{pr} + 7.661 - bT_{pr})^9, \tag{9}$$

$$P_{pr} = \frac{P}{7.386} + 4.20831\frac{T^{1.43}}{(c - T)(1 + 1.249P)}, \tag{10}$$

$$T_{pr} = \frac{1}{304.21}[T_{abs} - d(304.21 - T_{abs})], \tag{11}$$

$$T_{abs} = T + 273.15. \tag{12}$$

The values of coefficients a, b, c, and d in equations 8–11 are $a = 1.71$, $b = 7.789$, $c = 312$, and $d = 0$.

Figure 11 shows the modeled versus computed CO_2 velocity. This model is valid for the range of temperatures (from 25 °C to 200 °C) and pressures (from 20 MPa to 100 MPa) and is accurate to within an error of 1% except several temperature points from 50 °C to 100 °C and pressures below 40 MPa.

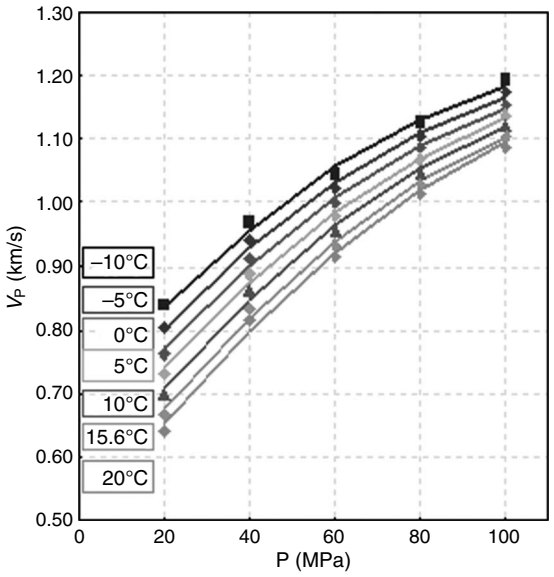

Figure 10. Calculated (solid lines) and measured (symbols) velocities of CO_2 as a function of pressure P for different LT from 20 °C to −10 °C.

CO_2 velocity model (LP) near the critical point

Because the LP range from 7 MPa to 20 MPa includes the CO_2 critical point, the velocity is very sensitive to temperatures and pressures. The form of equations 5–12 for the HT and HP range can be used to predict the velocity behavior of this LP range, but the values of coefficients a, b, c, and d in equations 8–11 are now $a = 1.66$, $b = 6.405$, $c = 30{,}000$, and $d = 40$.

The result shown in Figure 12 indicates they are almost matched within temperatures from 25°C to 40°C and the pressure range from 7 MPa to 13 MPa (not accurate near the critical point).

The results of comparing the measured CO_2 velocities to those calculated by these empirical models and by Span and Wagner's EOS (Span and Wagner, 1996) are shown in Figures 13 and 14. The EOS equation for CO_2 covers the wider temperature and pressure region from the triple-point temperature to 1100 K at pressures up to 800 MPa. The equation is accurate but contains many more terms. Some of the terms are complex exponentials that become difficult to evaluate accurately. Our new empirical models with fewer terms and a simple exponential are simpler and easier to implement. From Figure 14, we can see that at LT (e.g., < 100°C), the predicted velocity by the EOS model begins to deviate from the measured velocity trend at 50 MPa or lower. The new model is less accurate than Span and Wagner's in very LP regions but gives a more accurate prediction at elevated pressures.

Xu (2006) describes CO_2 properties by modifying Batzle-Wang's equations (Batzle and Wang, 1992). Compared to the laboratory-measured data by Wang and Nur (1989), Xu's calculated velocities produce a better match to the measured data than by using the original Batzle-Wang equations. We also applied our model to that same data set. A comparison of the measured and calculated results is shown in Figure 15, modified from the plot of Xu (2006). In Figure

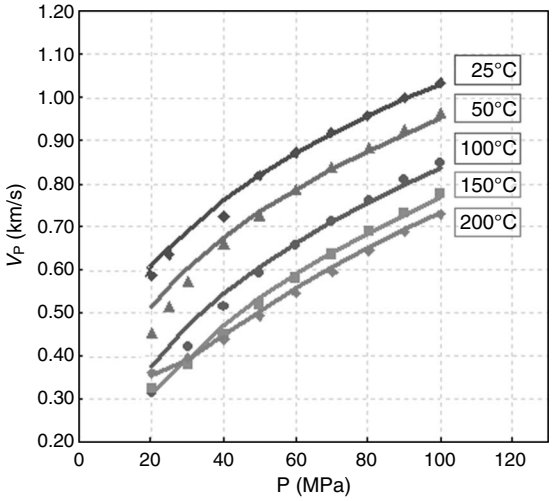

Figure 11. Calculated (solid lines) and measured (symbols) velocities of CO_2 as a function of pressure P for different temperatures from 25°C to 200°C.

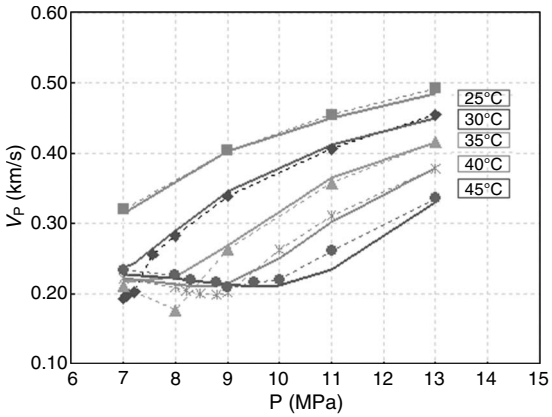

Figure 12. Calculated (solid lines) and measured (dashed lines) velocities of CO_2 as a function of pressure P for the range near the CO_2 critical point.

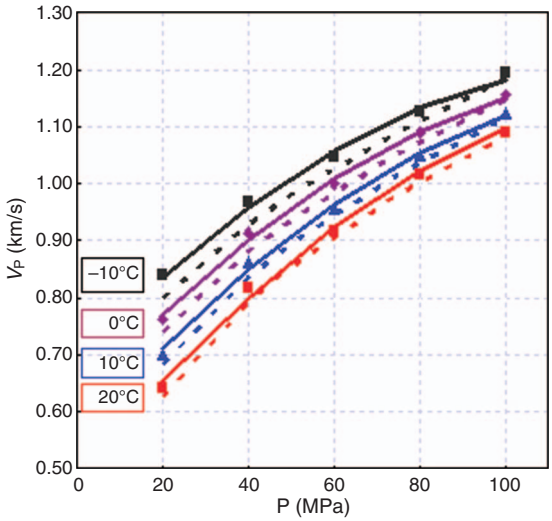

Figure 13. Comparing the calculated (solid lines based on the LTHP model) and measured velocities with the calculated velocities (dashed lines) by Span and Wagner (1996) for the LT and HP range.

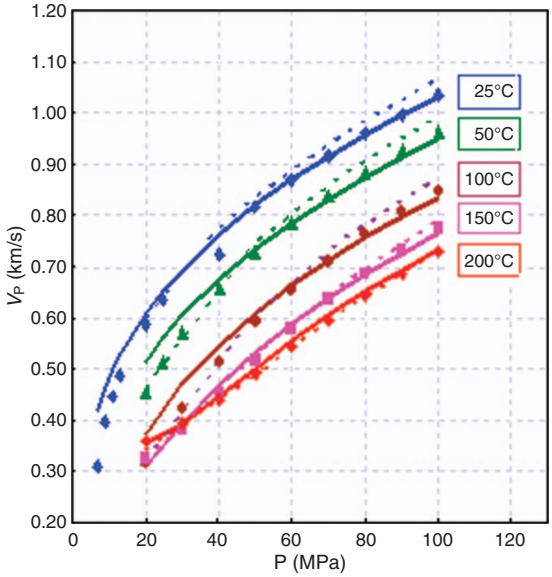

Figure 14. Comparing the calculated (solid lines based on the HTHP model) and measured velocities with the calculated velocities (dashed lines) by Span and Wagner (1996) for the HT and HP range.

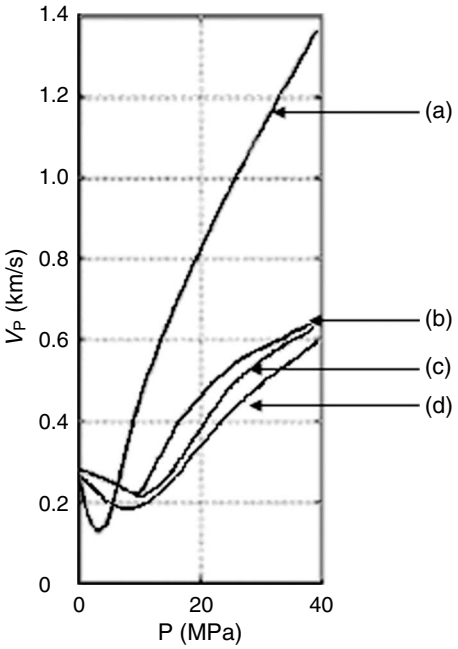

Figure 15. Comparing the calculated and measured CO_2 velocity: (a) Calculated velocity using Batzle-Wang equations; (b) calculated velocity using our model; (c) measured data by Wang and Nur (1989); (d) calculated velocity using Batzle-Wang's equations with modified parameters (Xu, 2006).

15, line a is calculated by using the original Batzle-Wang equations, line b is calculated by using our empirical model, line c represents measured data by Wang and Nur (1989), and line d is calculated by using Batzle-Wang equations with modified parameters by Xu (2006). It can be seen that our model matches the experimental data better when pressure is lower than the critical point (7.38 MPa) and higher than 25 MPa. Xu's results are better between approximately 10 MPa and 20 MPa.

CONCLUSION

We have carried out an experimental study of the acoustic velocity of CO_2 over a wide range of temperatures and pressures ($-10°C \le T \le 200°C$ and $7\ \text{MPa} \le P \le 100\ \text{MPa}$). In the HP range, $20\ \text{MPa} \le P \le 100\ \text{MPa}$, CO_2 is in a liquid-like state and velocities of CO_2 increase as pressure increases and temperature decreases. When pressure falls below 20 MPa with temperature in a range of 25–45°C, CO_2 approaches the critical point (31.1°C and 7.38 MPa) and its velocity is highly sensitive to temperature and pressure change. The velocities of CO_2 reach the minimum near the critical point. At pressures above the critical point, liquid-like behavior dominates (V_P decreases with increasing temperature). As pressures drop below the critical point, gas-like behavior dominates (V_P increases with increasing temperature).

We have developed velocity models of CO_2 based on the experimental data and described the relationships of CO_2 velocity with temperature and pressure. Generally, our models fit well with the experimental data. However, more laboratory data are needed to limit the bias of the experimental data and to refine the models, particularly in the critical region.

ACKNOWLEDGMENTS

This research has been supported by the Fluids/DHI consortium, which is sponsored by industry in collaboration with the University of Houston and the Colorado School of Mines.

REFERENCES

Bachu, S., 2000, Sequestration of CO_2 in geological media: Criteria and approach for site selection in response to climate change: Energy Conversion and Management, **41**, 953–970.
Batzle, M., and D. Han, 1998, Reservoir recovery processes and geophysics: The Leading Edge, **10**, 1444–1447.
Batzle, M., and Z. Wang, 1992, Seismic properties of pore fluids: Geophysics, **57**, 1396–1408.
Benson, S. M., P. J. Cook, J. Anderson, S. Bachu, H. B. Nimir, B. Basu, J. Bradshaw, G. Deguchi, J. Gale, G. von Goerne, W. Heidug, S. Holloway, R. Kamal, D. Keith, P. Lloyd, P. Rocha, B. Senior, J. Thomson, T. Torp, T. Wildenborg, M. Wilson, F. Zarlenga, D. Zhou, M. Celia, B. Gunter, J. E. King, E. Lindeberg, S. Lombardi, C. Oldenburg, K. Pruess, A. Rigg, S. Stevens, E. Wilson, S. Whittaker, G. Borm, D. Hawkins, and A. Lee, 2005, Underground geological storage of carbon dioxide, in Intergovernmental panel on climate change special report on carbon dioxide capture and storage: Cambridge University Press.
Duan, Z., N. Møller, and J. Weare, 1992, An equation of state for the CH_4–CO_2–H_2O system: I. Pure systems from 0 to 1000°C and 0 to 8000 bar: Geochimica et Cosmochimica Acta, **56**, 2605–2617.
Folas, G. K., E. W. Froyna, J. Lovland, G. M. Kontogeorgis, and E. Solbraa, 2007, Data and prediction of water content of high pressure nitrogen, methane and natural gas: Fluid Phase Equilibria, **252**, 162–174.
Han, D., and M. Batzle, 2000a, Velocity, density and modulus of hydrocarbon fluids — Data measurement: 70th Annual International Meeting, SEG, Expanded Abstracts, 1862–1866.
——, 2000b, Velocity, density and modulus of hydrocarbon fluids — Empirical modeling: 70th Annual International Meeting, SEG, Expanded Abstracts, 1867–1870.
Huber, M. L., 2007, NIST Thermophysical properties of hydrocarbon mixtures database (SUPERTRAPP) Version 3.2, U.S. Department of Commerce, National Institute of Standards and Technology.
Lazaratos, S. K., and B. P. Marion, 1997, Crosswell seismic imaging of reservoir changes caused by CO_2 injection: The Leading Edge, **16**, 1300–1306.
Majer, E. L., T. M. Daley, V. Korneev, D. Cox, J. E. Peterson, and J. Queen, 2006, Cost-effective imaging of CO_2 injection with borehole seismic methods: The Leading Edge, **25**, 1290–1302.
Onishi, K., T. Ueyama, T. Matsuoka, D. Nobuoka, H. Saito, and Z. Xue, 2007, Applying differential analysis to cross-well seismic survey for monitoring CO_2 sequestration: 77th Annual International Meeting, SEG, Expanded Abstracts, 2832–2836.
Shakhashiri, B. Z., 2008, General chemistry, http://www.scifun.org/CHEMWEEK/chemweek.html; accessed 23 December 2008.
Sijacic, D., K. H. A. A. Wolf, and J. Spetzler, 2008, Ultrasonic experiments for time-lapse monitoring of CO_2 sequestration: 78th Annual International Meeting, SEG, Expanded Abstracts, 3194–3198.
Skov, T., H. G. Borgos, K. A. Halvorsen, T. Randen, L. Sonneland, R. Arts, and A. Chadwick, 2002, Monitoring and characterization of a CO_2 storage site: 72nd Annual International Meeting, SEG, Expanded Abstracts, 1669–1673.
Span, R., and W. Wagner, 1996, A new equation of state for carbon dioxide covering the fluid region from the triple temperature to 1100 K at pressures up to 800 MPa: Journal of Physical and Chemical Reference Data, **25**, 1509–1596.
Wagner, W., and A. Kruse, 1998, Properties of water and steam: Springer-Verlag.
Walas, S. M., 1985, Phase equilibria in chemical engineering: Butterworth.
Wang, Z., and A. Nur, 1989, Effect of CO_2 flooding on wave velocities in rocks with hydrocarbons: Society of Petroleum Engineering Reservoir Engineering, **3**, 429–436.
Wang, Z., M. Cates, and R. Langan, 1998, Seismic monitoring of a CO_2 flood in a carbonate reservoir: A rock physics study: Geophysics, **63**, 1604–1617.
Xu, H., 2006, Calculation of CO_2 acoustic properties using Batzle-Wang equations: Geophysics, **71**, no. 2, F21–F23.
Xue, Z., D. Tanase, H. Saito, D. Nobuoka, and J. Watanabe, 2005, Time-lapse crosswell seismic tomography and well logging to monitor the injected CO_2 in an onshore aquifer, Nagaoka, Japan: 75th Annual International Meeting, SEG, Expanded Abstracts, 1433–1436.
Zhang, Y., 2005, Fate of rising CO_2 droplets in seawater: Environmental Science and Technology, **39**, 7719–7724.